Geochemistry Geophysics Geosystems G3

Article
Volume 13, Number 11
2 November 2012
Q11001, doi:10.1029/2012GC004305
ISSN: 1525-2027

Published by AGU and the Geochemical Society

Petrophysical and geochemical properties of Columbia River flood basalt: Implications for carbon sequestration

Natalia V. Zakharova and David S. Goldberg
Borehole Research Group, Lamont-Doherty Earth Observatory, Columbia University, 61 Route 9W, Palisades, New York 10964, USA (nzakh@ldeo.columbia.edu)

E. Charlotte Sullivan
Pacific Northwest National Laboratory, 902 Battelle Boulevard, Richland, Washington 99352, USA

Michael M. Herron and James A. Grau
Schlumberger-Doll Research, 1 Hampshire Street, Cambridge, Massachusetts 02139, USA

[1] This study presents borehole geophysical data and sidewall core chemistry from the Wallula Pilot Sequestration Project in the Columbia River flood basalt. The wireline logging data were reprocessed, core-calibrated and interpreted in the framework of reservoir and seal characterization for carbon dioxide storage. Particular attention is paid to the capabilities and limitations of borehole spectroscopy for chemical characterization of basalt. Neutron capture spectroscopy logging is shown to provide accurate concentrations for up to 8 major and minor elements but has limited sensitivity to natural alteration in fresh-water basaltic reservoirs. The Wallula borehole intersected 26 flows from 7 members of the Grande Ronde formation. The logging data demonstrate a cyclic pattern of sequential basalt flows with alternating porous flow tops (potential reservoirs) and massive flow interiors (potential caprock). The log-derived apparent porosity is extremely high in the flow tops (20–45%), and considerably overestimates effective porosity obtained from hydraulic testing. The flow interiors are characterized by low apparent porosity (0–8%) but appear pervasively fractured in borehole images. Electrical resistivity images show diverse volcanic textures and provide an excellent tool for fracture analysis, but neither fracture density nor log-derived porosity uniquely correlate with hydraulic properties of the Grande Ronde formation. While porous flow tops in these deep flood basalts may offer reservoirs with high mineralization rates, long leakage migration paths, and thick sections of caprock for CO_2 storage, a more extensive multiwell characterization would be necessary to assess lateral variations and establish sequestration capacity in this reservoir.

Components: 12,100 words, 9 figures, 2 tables.

Keywords: Columbia River basalt; borehole geophysics; carbon sequestration; geochemical logging.

Index Terms: 0915 Exploration Geophysics: Downhole methods; 1699 Global Change: General or miscellaneous; 1859 Hydrology: Rocks: physical properties.

Received 21 June 2012; **Revised** 27 September 2012; **Accepted** 30 September 2012; **Published** 2 November 2012.

Zakharova, N. V., D. S. Goldberg, E. C. Sullivan, M. M. Herron, and J. A. Grau (2012), Petrophysical and geochemical properties of Columbia River flood basalt: Implications for carbon sequestration, *Geochem. Geophys. Geosyst.*, *13*, Q11001, doi:10.1029/2012GC004305.

1. Introduction

[2] Geologic storage of carbon dioxide (CO_2) provides a vital option to mitigate climate change by reducing anthropogenic CO_2 emissions into the atmosphere [*Intergovernmental Panel on Climate Change*, 2005]. In a number of recent studies, igneous rocks were identified as a promising target for carbon dioxide storage [e.g., *Goldberg et al.*, 2010; *Matter et al.*, 2007; *McGrail et al.*, 2006]. Unlike sedimentary aquifers where CO_2 is primarily contained by a caprock or by dissolution in formation water [e.g., *Bachu*, 2008; *Lackner*, 2003], igneous rocks have high potential for mineral trapping, which results in permanent binding of injected CO_2 into carbonate minerals [*Matter and Kelemen*, 2009]. Thus, mineral trapping via carbonation may provide the most secure CO_2 underground storage over the long-term. Studies of natural analogs and laboratory experiments suggest that mineralization reactions may happen relatively quickly (years to centuries), and thousands of tons of CO_2 can be converted to carbonates each year [e.g., *Dessert et al.*, 2003; *Kelemen and Matter*, 2008; *McLing et al.*, 2009; *Schaef et al.*, 2010].

[3] Among various igneous rocks, basalts have received much attention due to their widespread occurrence and potentially suitable reservoir structures [*Goldberg et al.*, 2008; *Matter et al.*, 2009]. In particular, continental flood basalts such as the Columbia River Plateau, Siberian or Deccan traps possess large storage capacity for carbon dioxide injection [*McGrail et al.*, 2006]. They represent massive successions of extensive basalt flows and occur all over the globe [*Bryan and Ernst*, 2008]. The majority of flows have porous outer regions, formed during rapid cooling and degassing, that can serve as reservoirs for anthropogenic carbon dioxide. At the same time, interbedded sediment layers and dense low-permeability inner-flow sections can be effective seals allowing time for mineralization reactions to occur [*Goldberg et al.*, 2010]. *McGrail et al.* [2006] estimated the CO_2 storage potential of the Columbia River Basalt Group (CRBG) to exceed 100 Gt, which is enough to store the entire emissions of the northwestern U.S. for the foreseeable future.

[4] The Wallula pilot CO_2-sequestration project was established to evaluate the potential of continental flood basalt sequestration through a small-scale (1000 metric tons) field injection experiment [*McGrail et al.*, 2011]. One 1253-m borehole was drilled through the CRBG in Walla Walla County in southeastern Washington, and extensive geophysical, geochemical, hydrologic, and microbiologic surveys were carried out by Battelle, in collaboration with Big Sky Regional Carbon Sequestration Partnership and Boise Inc [*McGrail et al.*, 2009]. Based on hydraulic testing conducted during drilling and immediately thereafter, the target injection zone was identified at 828–887 m spanning three brecciated interflow zones (Ortley and Slack Canyon 2–3 member flow tops) that represent a single hydraulic unit with relatively high permeability bounded by thick low-permeability flow interiors (i.e., caprock intervals). Detailed description of the site selection, the injection zone and caprock characterization, and the planned post-injection activities are reported by *McGrail et al.* [2009] and are summarized by *McGrail et al.* [2011]. As one of the first detailed-characterized boreholes for deep CRBG in the region, the Wallula pilot offers a unique chance to improve the general understanding of flood basalt properties in the context of CO_2 storage. This study analyzes the full suite of geophysical data available from the Wallula borehole, including the now-cemented interval below the target injection zone, with a broader objective of improving the knowledge of the capabilities and limitations of well logging in basaltic rocks for site characterization and CO_2-injection monitoring.

[5] Geophysical logging provides a useful tool for formation evaluation, critical for assessing reservoir properties and seal integrity, and establishing baseline (pre-injection) conditions for the further monitoring of CO_2 underground. Due to unconventional lithology and complex formation structure, basaltic formations pose additional challenges for petrophysical analysis, and require formation-specific processing and calibration of the logging data to core measurements. This paper presents specifically processed borehole geophysical data and new geochemistry analysis of the sidewall core from the Wallula borehole, and provides petrophysical and geochemical characterization for the Grande Ronde Basalt. The use of geochemical logs, which are rarely acquired in volcanic rocks, is evaluated with unique processing parameters for these igneous lithologies, and allows for a vertically continuous geochemical characterization of the Grande Ronde Basalt. To the best of our knowledge, this is the first example of neutron capture spectroscopy logging in the Columbia River Basalt Group. With this study, the ability of spectroscopy logging to detect secondary mineralization in the CRBG can be established. Since mineral trapping is expected to provide a secure mechanism for long-term CO_2 storage in

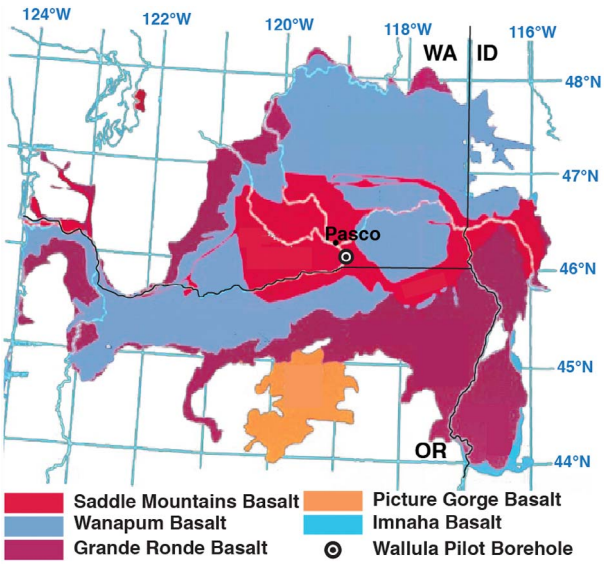

Figure 1. The study site location and the areal extent of the five basalt formations in the Columbia River Basalt Group (modified from *Reidel et al.* [2002]).

basalt, such techniques for measurement of in situ carbonate precipitation may become a key aspect of post-injection monitoring, verification and accounting.

2. Background Information

2.1. Regional Setting

[6] The Columbia River Basalt Group is a continental flood basalt province that covers over 200,000 km^2 of the Pacific Northwest in Washington, Oregon and Idaho (Figure 1) [*Hooper*, 2000; *Reidel et al.*, 2002]. The flood basalts erupted from linear fissures between 17.5 and 6 Ma ago (late Miocene-early Pliocene), but the majority of flows formed during a period of only 2.5 million years (17–14.5 Ma ago) [*Martin et al.*, 2005]. The CRBG consists of a sequence of a few hundred tholeiitic basalt flows with a total estimated volume of approximately 224,000 km^3. During the time of peak activity, many individual flows exceeded 1,000 km^3 in volume, and traveled hundreds of kilometers from their vent system [*Tolan et al.*, 1989]. The CRBG flows typically consist of a permeable flow top, a dense, relatively impermeable flow interior, and a flow bottom of variable thickness [*Department of Energy* (*DOE*), 1988]. Flow tops usually consist of a chilled, glassy crust that is often vesicular to scoriaceous, or rubbly to brecciated (hereafter referred to as porous and brecciated flow tops). The bottom part of the flow may also consist of a glassy, vesicular zone that is typically a few centimeters thick, although thickness may vary. The collective contact boundary section between two individual basalt flows, i.e., a flow top and an overlying flow bottom, is referred to as an interflow zone. The flow interior (also referred to as the inner flow) may include massive basalt and/or multiple layers of colonnades and entablatures. The colonnade refers to well-defined columnar structures oriented perpendicularly to flow boundaries and typically occurring in the basal portion of the flow, but which may also constitute its entire thickness or form at several levels, alternating with entablatures. Entablatures are characterized by greater abundance of cooling joints that are more randomly oriented [*Long and Wood*, 1986]. Interbedded sedimentary layers and basalt interflow zones serve as the primary aquifers in the region, while dense flow interiors commonly act as aquitards [*Reidel et al.*, 2002].

[7] Despite their huge volumes and great lateral extent, the stratigraphic units in the CRBG can be reliably identified and correlated on a regional basis, mostly due to the remarkable geochemical homogeneity of individual flows [*Hooper*, 2000]. Based on the combination of geochemical composition, paleomagnetic properties, and lithology, the CRBG is divided into six formations (in ascending stratigraphic order): the Imnaha, Grande Ronde, Picture Gorge, Prineville, Wanapum, and Saddle Mountains Basalt, each of which is further subdivided in members and flows [e.g., *Reidel*, 1998]. The Grande Ronde Basalt, which erupted 16.5 to 14.5 Ma ago, makes up about 85% of the CRBG by volume, and consists of 17 individual members [*Reidel et al.*, 1989]. It was identified as a target formation for CO_2 injection based on its great cumulative thickness, suitable depths and hydraulic properties [*Spane et al.*, 2007].

2.2. Site Description

[8] The Wallula pilot borehole is located approximately 20 km southeast of Pasco in western Walla Walla County in southeastern Washington (Figure 1), where the CRBG has the greatest aggregate thickness of more than 3 km [*Spane et al.*, 2007]. The test hole is 1253 m deep, about 31.1 cm in diameter, and almost vertical (15.2 m cumulative deviation at the bottom of the borehole in the northeastern direction). Logging was conducted in the open section from 337.72 m to the bottom of the hole. The stratigraphy of the Wallula borehole was established based on regional geologic correlation, X-Ray fluorescence (XRF) analysis of drilling cuttings, and field logging data [*McGrail et al.*,

2009]. The Wallula pilot borehole intersects three CRBG formations: Saddle Mountain, Wanapum and Grande Ronde (in descending order). This study focuses on the Grande Ronde Basalt, the target formation for CO_2 storage [*McGrail et al.*, 2006].

[9] The CRBG lithology is dominated by clinopyroxene, plagioclase, and glassy mesostasis [*Reidel*, 1983]. Clinopyroxene is mostly augite, with pigeonite as an accessory phase. A minor amount of orthopyroxene (enstatite bronzite to hypersthene) is also present, and olivine content is low (0–3%). Accessory minerals include hematite, apatite, ilmenite, and magnetite. Glass content ranges from a few percent to over 50%. Secondary minerals are represented by smectite, clinoptilolote, celadonite, opal, pyrite, and minor amount of calcite [*Horton*, 1991; *Porter*, 2010].

3. Data and Methods

3.1. Standard Wireline Logging

[10] Wireline logging data were collected by Schlumberger in the open section of the Wallula borehole (340–1250 m) following drilling and preliminary well completion. The data include caliper (borehole diameter), total natural gamma radioactivity, bulk density, thermal neutron porosity, electric resistivity, sonic velocities, and borehole spectroscopy. All logs were corrected for geometrical borehole effects, checked for measurement quality, and recalibrated for the basalt formation matrix when necessary. Overall, log data quality was excellent. Apparent electric resistivity was recorded by Array Induction Imager Tool™ (AIT™) as a function both of depth and penetration radius into the formation (0, 25, 50, 75, 150 and 230 cm), with vertical resolution of up to 30 cm. The 25-cm penetration channel exceeded the AIT measurement scale in many zones due to high contrast between nearly fresh borehole water and the formation resistivity. Other channels were not affected. High-resolution resistivity images of the borehole wall were recorded using the Fullbore Formation MicroImager™ (FMI™). These images, generated from 192 microresistivity sensors located on four orthogonal tool arms, allow for azimuthal data analysis and have a maximum vertical and azimuthal resolution of 0.5 cm. The azimuthal coverage of the FMI sensors in a 31.1-cm borehole is about 50%. Processed electric resistivity images were used for flow structure and fracture analysis. Sonic velocities of compressional and shear waves were computed from full waveform transit times and displayed high coherency and reliability throughout the interval. Caliper, total gamma ray, density, electrical and sonic logs were primarily used for establishing flow boundaries and wellbore stratigraphy, in combination with XRF chemistry analysis from cuttings reported in *McGrail et al.* [2009].

[11] To estimate porosity, a combination of four different logging methods was used (i.e., density, neutron, sonic and electric resistivity) [*Ellis and Singer*, 2007]. Raw porosity logs (density, neutron and sonic) disagreed by as much as 20% (i.e., 20 porosity units), contained some unrealistic (e.g., negative) values, and therefore, required reprocessing and core calibration. No core porosity measurements were available at the site; thus, log-derived porosity was computed using physical properties of the basalt matrix. Matrix density was measured on 12 sidewall cores selected for chemistry analysis (see auxiliary material).[1] The average grain density for the 7 samples from the massive inner flows (2.90 g/cm^3) was assumed to be the matrix density value. Density porosity was calculated using the weighted-average transform and core matrix density [*Schlumberger*, 1989]. The sonic P wave velocity of the matrix (6.1 km/s) was obtained from a density-velocity crossplot, and was in good agreement with published values for basalt [e.g., *Boldreel*, 2006; *Broglia and Moos*, 1988]. An empirical velocity-porosity transform [*Raymer et al.*, 1980] best fit these data and was used instead of the Wyllie time-average equation. For resistivity-based porosity estimates, the deep-reading resistivity log (230 cm penetration) and Archie coefficients of a = 0.1 and m = 2, derived from the density porosity-resistivity crossplot, produced the best fit formation factor. These values also agree with previous studies in basalts [e.g., *Goldberg and Burgdorff*, 2005; *Pezard*, 1990]. Finally, the thermal neutron log, which commonly overestimates porosity values due to strong sensitivity to clays and formation water salinity [*Broglia and Ellis*, 1990], was recalibrated to match density porosity values by applying a static −5% correction.

3.2. Borehole Spectroscopy Logging and Geochemical Analysis

[12] Borehole geochemical logging based on neutron-induced gamma ray spectroscopy allows evaluation of elemental concentrations of several key rock-forming elements as continuous functions of depth [e.g., *Anderson et al.*, 1990; *Grau and*

[1] Auxiliary materials are available in the HTML. doi:10.1029/2012GC004305.

Table 1. Oxide Association Factors Used in the Closure Model for the ECS Processing

Element	Pure Oxides	Volcanic Closure Model
Si	2.139	2.139
Al	1.889	1.889
Ca	1.399	1.830
Mg	1.658	2.480
Na	1.348	1.348
K	1.205	1.760
Fe	1.430	1.430
Ti	1.668	1.668
S	1.998	0.064

Schweitzer, 1989; *GuoXin et al.*, 2007]. A neutron capture spectroscopy tool emits fast (i.e., high energy) neutrons and measures the energy spectrum of gamma rays generated by a variety of interactions between neutrons and atomic nuclei, including inelastic scattering and neutron capture [*Ellis and Singer*, 2007]. The geochemical logging data in the Wallula borehole were recorded with the Elemental Capture Spectroscopy™ (ECS™) sonde. The tool has an americium beryllium (AmBe) neutron source (peak energy about 4.2 MeV), and a large, bismuth germanate (BGO) detector recording a 254-channel gamma ray spectrum. The gamma rays induced by neutron capture comprise most of the recoded spectrum, however, inelastic neutron-nucleus interactions also contribute to the signal. For the ECS tool, the inelastic spectrum is accounted for during processing but it is not analyzed quantitatively. The ECS tool provides concentrations primarily of elements with high neutron capture cross-section: gadolinium (Gd), chlorine (Cl), barium (Ba), titanium (Ti), iron (Fe), calcium (Ca), silicon (Si), sulfur (S), and hydrogen (H). With customized processing, the potassium (K), aluminum (Al), and magnesium (Mg) concentrations may also be estimated.

[13] An ECS gamma ray spectrum includes contributions from the elements found both in the formation and the borehole. Fluids filling a large diameter borehole or abundant zones with high porosity can result in a high hydrogen contributions (up to 40% of the spectrum in the Wallula ECS data), leading to a lower sensitivity to some key elements in the rock matrix. In order to obtain elemental concentrations of the rock matrix, the contribution of the formation water (H and Cl) must be subtracted, and the residual spectrum be decomposed into the relative proportions, or relative yields, of contributing elements through a process of spectral stripping that utilizes standardized spectra of the contributing elements [*Grau and Schweitzer*, 1989]. These relative yields are functions of the amounts present in the formation and the measurement sensitivity to each element. Elemental concentrations are ultimately obtained by applying an oxide closure model that accounts for the remaining unmeasured elements in the formation, such as oxygen.

[14] Due to the complex chemical composition of the volcanic rock-forming minerals, and the occurrence of major elements in solid solutions, some element-to-oxygen ratios in basalt are different from those in pure oxides. These ratios should be determined from chemical analysis on cores. Due to a limited amount of core chemical analysis in the Wallula pilot borehole, an oxide closure model specifically developed for a volcanic reservoir was used, as shown in Table 1 [*GuoXin et al.*, 2007]. This model was obtained by multiple regression optimization of chemical analyses on 98 core samples from the YingCheng Group in northeastern China, characterized by a wide range of volcanic lithologies. Chemical composition data available from sidewall cores in the Wallula pilot borehole matched the YingCheng model chemistry well.

[15] Sidewall rotary minicores were collected in the Wallula pilot borehole using a wireline tool after the completion of drilling and logging operations. The sidewall cores are 2.5 cm in diameter, and about 2–5 cm long, with varying sample recovery (Figure 2). Five cores were selected from flow tops, and 7 from inner flows for chemical analysis. A portion of each sample was crushed and split into several aliquots. No effort was made to clean the samples from potential drilling mud contamination to avoid eliminating natural clay minerals. A 12 g sample was analyzed for elemental composition at SGS Mineral Services (Toronto) for major oxides (XRF), 55 elements (ICP-OES and ICP-MS), total sulfur (Leco), total carbon (Leco), organic carbon (coulometry), CO_2 (coulometry), FeO (titration), H_2O+ (Penfield). A 1 g sample was allocated for grain density measurements using a pycnometer (Micromeritics). The resulting major and minor cation concentrations from the core analyses were used to estimate the accuracy of the ECS logs. The full chemical analysis on these samples is available in the auxiliary material.

[16] A multivariate factor analysis was employed to statistically handle the chemical data and to find simplifying relationships. Factor analysis is capable of resolving distinct patterns in data by interpreting the statistical structure of the variance-covariance matrix [*Reidel*, 1983]. A minimum number of new

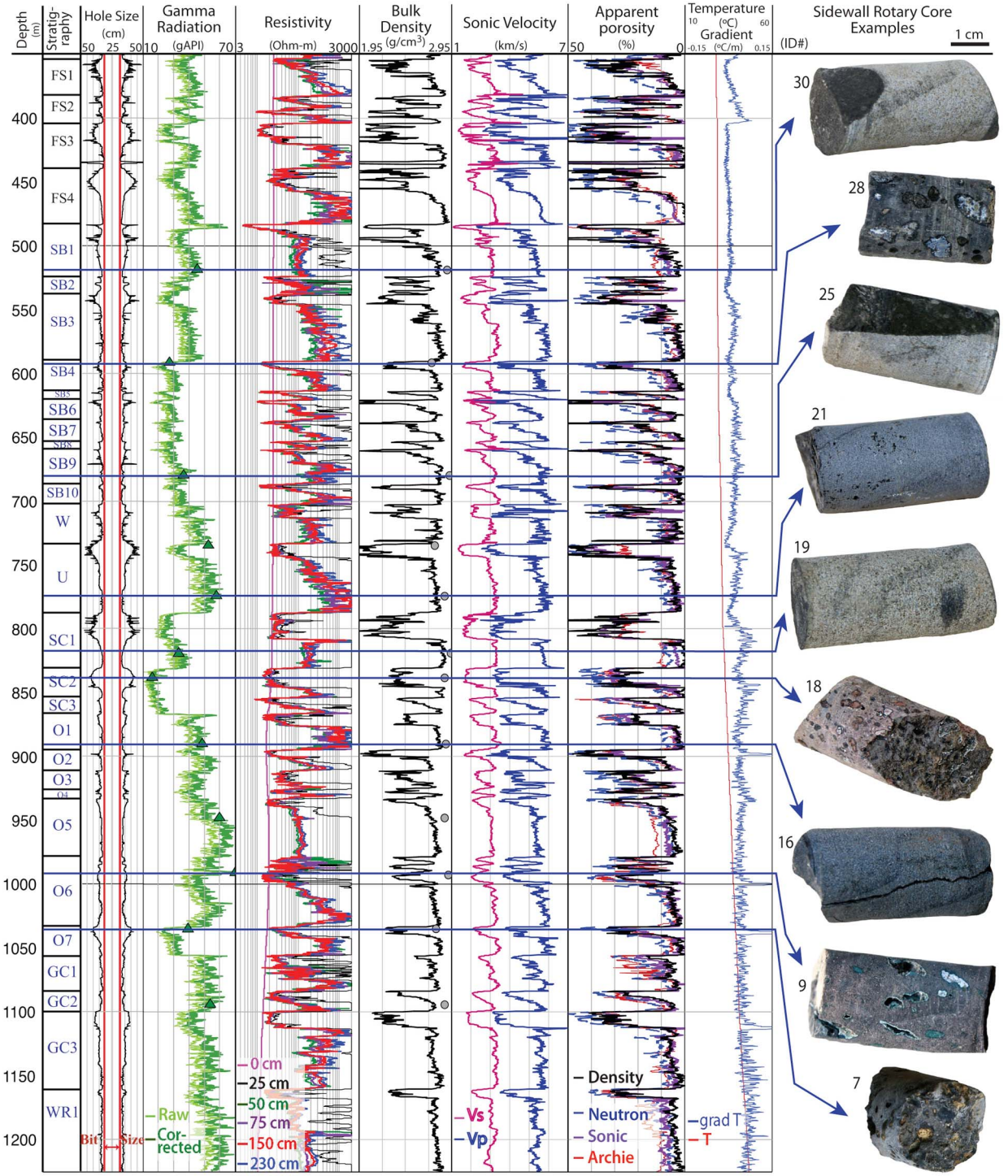

Figure 2. Processed logging data and examples of sidewall cores from the Wallula borehole, illustrating alternating flow tops and flow interiors. Resistivity logs are color-coded according to the depth of penetration into formation away from the borehole. Triangles indicate natural gamma ray values predicted from sidewall core chemistry. Grey dots represent matrix density measured on the samples. Stratigraphy is revised from *McGrail et al.* [2009], and flow members are indicated as following: FS – Frenchmen Springs, SB – Sentinel Bluffs, W – Winterwater, U – Umtanum, SC – Slack Canyon, O – Ortley, GC – Grouse Creek, WR – Wapshilla Ridge (the Wanapum formation members are labeled in black, the Grande Ronde members in blue).

variables – factors – are created by linear recombination of the original data. Only factors that account for more variance than the original input data are retained (using the criterion for unrotated eigenvalues being greater than unity). For this study, R-mode factor analysis with varimax rotation [*Davis*, 1986] was performed to reveal underlying relationships between elemental concentrations in the core and log data sets.

4. Results

4.1. Volcanostratigraphy and Petrophysical Properties

[17] Two distinct lithofacies are identified from the wireline logs. Brecciated vesicular basalt is characterized by low density, electric resistivity and sonic velocity; massive basalt is characterized by high values of these measurements and approaches the nominal values for basaltic matrix (Figure 2). On average, the compressional velocity in the massive Grande Ronde Basalt is 5.5–6 km/s and shear velocity is about 3.5 km/s. Sonic velocities in vesicular basalt are about 50% of the values in massive basalt. Massive basalt has high electrical resistivity ranging from 200 to 2,000 Ohm-m at different depths. This order-of-magnitude variation is attributed to varying extents of fracturing in the CRBG, as described below. Apparent resistivity in vesicular basalt intervals is 1–2 orders of magnitude lower, 10–20 Ohm-m on average, and close to the resistivity of the borehole fluid. The bulk density of massive units is about 2.8–2.9 g/cm^3, close to the density of the basalt matrix, while bulk density in vesicular units reaches as low as 1.9 g/cm^3. This dramatic difference in bulk density is due primarily to variations in the porosity; however, the presence of low-density hydrous minerals in the rock matrix may also contribute. Grain density measured on sidewall cores is lower in the vesicular units than in massive basalt, 2.82 $\pm$ 0.08 g/cm^3 and 2.90 $\pm$ 0.03 g/cm^3, respectively. The vesicular intervals are also characterized by distinct washouts in the borehole, indicated by the caliper log (Figure 2). Visual observations of the sidewall cores also indicate two distinct lithofacies penetrated by the borehole: massive basalts (some with fractures), gray to black in color, with high grain density, and high sample recovery; and highly altered porous basalt, with varying color, partial mineralized infilling materials, lower grain density, and incomplete recovery. The massive units are interpreted to represent the inner portions of basaltic flows that cooled slowly over time whereas the vesicular units correspond to porous and brecciated interflow zones formed by rapid cooling and degassing of sub-aerial flows [*McGrail et al.*, 2009].

[18] The wireline log data show a consistent cyclic pattern of sequential basalt flows with alternating porous interflow zones and massive inner flow units. Twenty-six flows from 7 members of the Grande Ronde formation were intersected by the pilot borehole and are identified in the logs, refining the resolution of the XRF-based stratigraphy reported by *McGrail et al.* [2009]. The flows vary in thickness from 10 to 70 m, with porous flow tops ranging from 3 to 20 m thick. A comparison of the XRF-based stratigraphy to the logs suggests that all of the Grande Ronde flows intersected by the borehole have high-porosity flow tops. The apparent porosity logs all estimate extremely high values of 20% to 50% in these flow tops. Drilling damage and uncorrected clay effects may bias these values, but their thicknesses can be accurately measured. The thickest flow tops occur in the Grouse Creek 3, Slack Canyon 1 and 2, and Umtanum flows. Flow interiors are characterized by 0–10% porosity, and often exhibit a porosity gradient from high values immediately below the flow tops to near-zero in the bottom part of the flows. Overall, higher porosity values (~5–10%) correspond to higher planar fracture density observed in resistivity images, while near-zero porosity tend to occur in massive basalt at the base of a few flows in the section (Figure 2).

[19] High-resolution FMI images reveal diverse volcanic textures and dense fracturing in the majority of the flows. Most of the flow boundaries are marked by a sharp change from a massive flow bottom to a brecciated flow top. Similar observation has also been made in CRBG outcrops (Figure 3a). No distinct porous zones were observed in the images of flow bottoms, suggesting that the glassy crust at the bottom boundaries is either very thin or indistinguishable from the underlying flow tops. Transitions from the brecciated flow tops to dense flow interiors are usually gradual, reflecting gradual cooling away from the exposed upper boundary after flow emplacement, while bottom boundaries appear sharp in the FMI images. This suggests that the interflow zones in the Wallula pilot borehole are dominated by flow tops. Flow boundaries are subhorizontal, and do not have a dominant dip azimuth. The slight variations in orientation of flow boundaries were likely controlled by local topography at the time of individual flow emplacement. All flow tops exhibit similar vesicular, rubbly and brecciated textures. Flow interior structures are very diverse, however, with complex patterns of fractures and

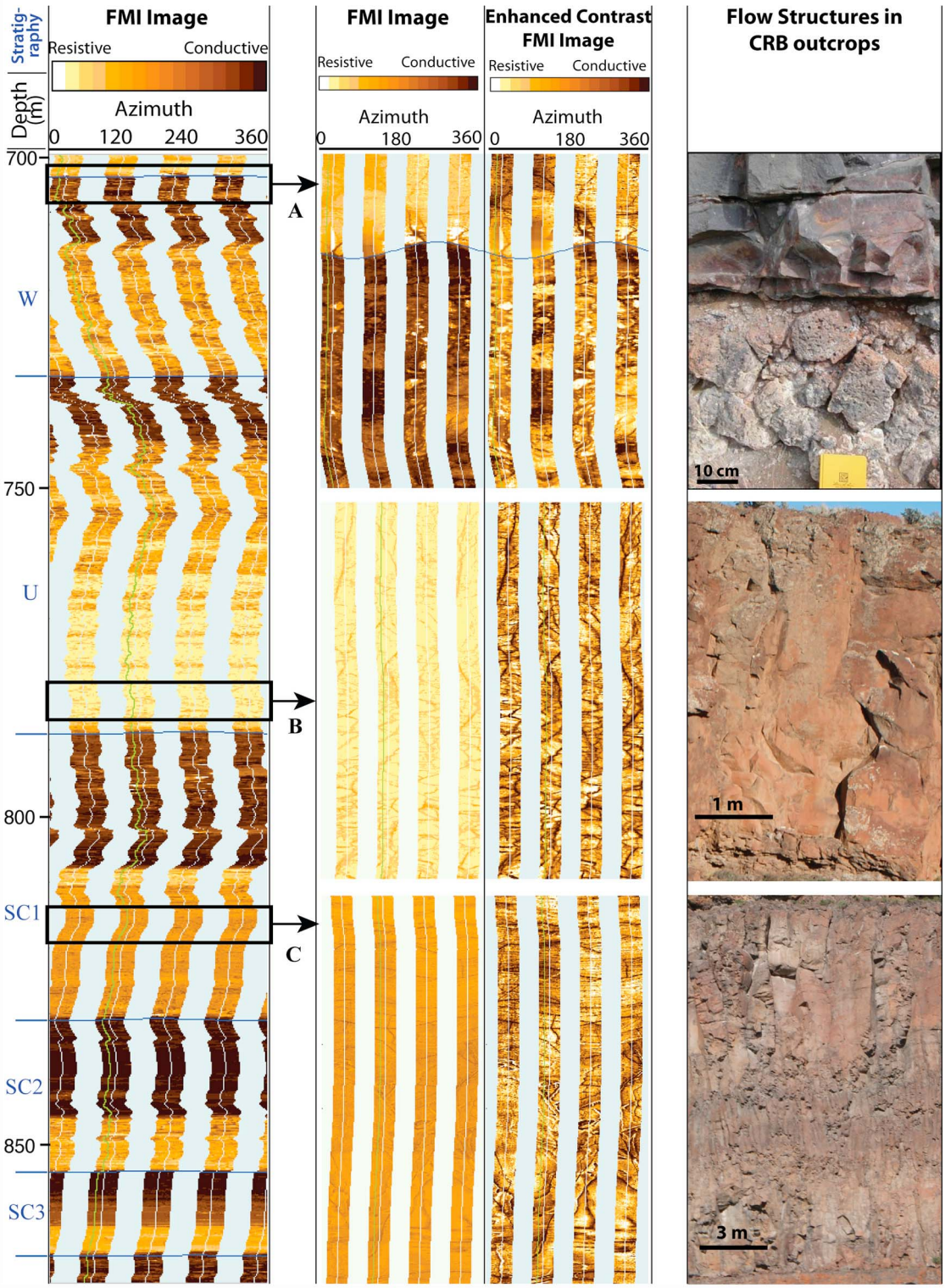

Figure 3. Electric resistivity (FMI) images of the borehole walls compared to the large-scale features observed in the Columbia River Basalt outcrops: (a) Flow boundary exhibiting sharp contrast between massive flow bottom and a brecciated flow top (the photograph credits: K. Davis and C. Porter); (b) Massive basalt, with drilling-induced fractures in the FMI images, (c) Inner-flow entablature and colonnades with abundant cooling joints. (The outcrops images illustrate the suggested interpretation of the flow structures observed in the FMI images, and do not correspond to the specific flow members intersected by the borehole.)

cooling joints. Two major electrofacies can be distinguished in the flow interiors: 1) moderate resistivity zones (100–500 Ohm-m), with abundant planar fractures (Figure 3c) and no separation between resistivity curves, and 2) high resistivity zones (over 1000 Ohm-m), characterized by complex network of vein-like fractures (Figure 3b) and by significant separation between deep- and shallow-penetrating resistivity logs. The moderate resistivity zones are much more common in the section, and correspond to fractured flows with developed entablatures and colonnades. Entablatures are volumetrically most significant in the CRBG outcrops, and comprise 60–70% of the exposed Grande Ronde flows [e.g., *Long and Wood*, 1986]. They have relatively irregular fracture patterns that form uneven columns 0.2–0.5 m in diameter. Colonnades are less common in the CRBG (10–30%), and have well defined columns 0.3–2 m in diameter. A single borehole 30–40 cm in diameter does not provide enough spatial coverage to unambiguously distinguish between these two flow structures. However, moderate resistivity values and an abundance of conductive fractures suggest that the moderate resistivity electrofacies contains extensive jointing common for entablatures and that some of the fractures are open (water or clay-filled). The high-resistivity zones are less abundant, and occur in less than 30% of the flows (e.g., the Umtanum member, Ortley 1, and narrow zones in the Sentinel Bluffs and Grouse Creek flows). A positive gradient in resistivity away from the borehole suggests that vein-shaped conductive features common for these zones are confined to the vicinity of the borehole, and are likely caused by drilling-induced damage. The high resistivity electrofacies most likely represents massive basalt (potentially with closed joints) and/or large-diameter colonnades. The relative position and abundance of the two electrofacies supports this interpretation: the moderate resistivity fractured zones are found below flow tops and they exist in the majority of the flows, while the high-resistivity massive basalt occurs only in the deepest part of a few flow interiors (e.g., the Umtanum member (733–788 m) in Figure 3). This may be interpreted as slow cooling and little or no jointing in the deep flow interior with progressive cracking upwards where cooling progressed more quickly.

[20] In the FMI images, the orientation of conductive, planar fractures changes with depth, but the predominant strike direction is NW-SE with the dip angles from 10 to 80 degrees. Figure 4a illustrates that shallow dipping cracks are more randomly oriented. These likely represent sub-horizontal cooling joints that form in bands normal to the sub-vertical columns, a common feature in columnar basalts [e.g., *DeGraff and Aydin*, 1987]. Figure 4b indicates that high-angle fractures (60–80 degrees) tend to dip to the northeast, most likely formed by tectonic processes after emplacement and cooling. This orientation is consistent with the maximum horizontal compressive stress oriented NW-SE at the time of fracturing, but does not rule out other explanations. The regional stress direction has been estimated from earthquake focal mechanisms in southeastern Washington and is available from the World Stress Map database [*Heidbach et al.*, 2008]. The two estimates of the maximum horizontal stress in the area differ – from NW-SE to NE-SW azimuth (Figure 4c) – and more data are needed to reconcile them. Borehole breakouts are absent in the Wallula FMI images, but an earlier study at the Hanford site (about 70 km away) reported clear borehole breakouts in the E-W direction, indicative of the N-S maximum horizontal stress (Figure 4d) [*Paillet and Kim*, 1987]. Other data in the Pasco basin, including hydraulic fracturing tests and microseismic focal mechanisms also indicate a north-south orientation of the maximum horizontal stress and a near-vertical minimum stress [*DOE*, 1988]. Moreover, regional geologic evidence suggests that this stress regime has existed for the past 14.5 Ma [*DOE*, 1988]. Therefore, the steeply dipping tectonic fractures were likely formed under the dominant N-S horizontal compressive stress through a combination of strike-slip and thrust mechanisms. *Sullivan et al.* [2011] showed that the fast direction of shear wave anisotropy from the sonic log is primarily NW, with a minor E-W component. Intrinsic formation properties such as fracture orientation, as well as the current stress regime may contribute to shear wave anisotropy. In this case, the observed shear wave anisotropy is interpreted as primarily caused by the fracture alignment rather than by active regional horizontal stresses.

4.2. Chemical Composition and Borehole Spectroscopy

[21] The total gamma ray (GR) activity corresponding to Th, U and K concentrations ranges from about 20 API to 80 API, and is close to 50 API in most flows (Figure 2). The Sentinel Bluffs 4–9 members (590–690 m), the Slack Canyon member (790–867 m, near the target injection zone) and the Ortley 7 member (1036–1056 m) have the lowest natural GR activity. Some of the low-GR intervals coincide

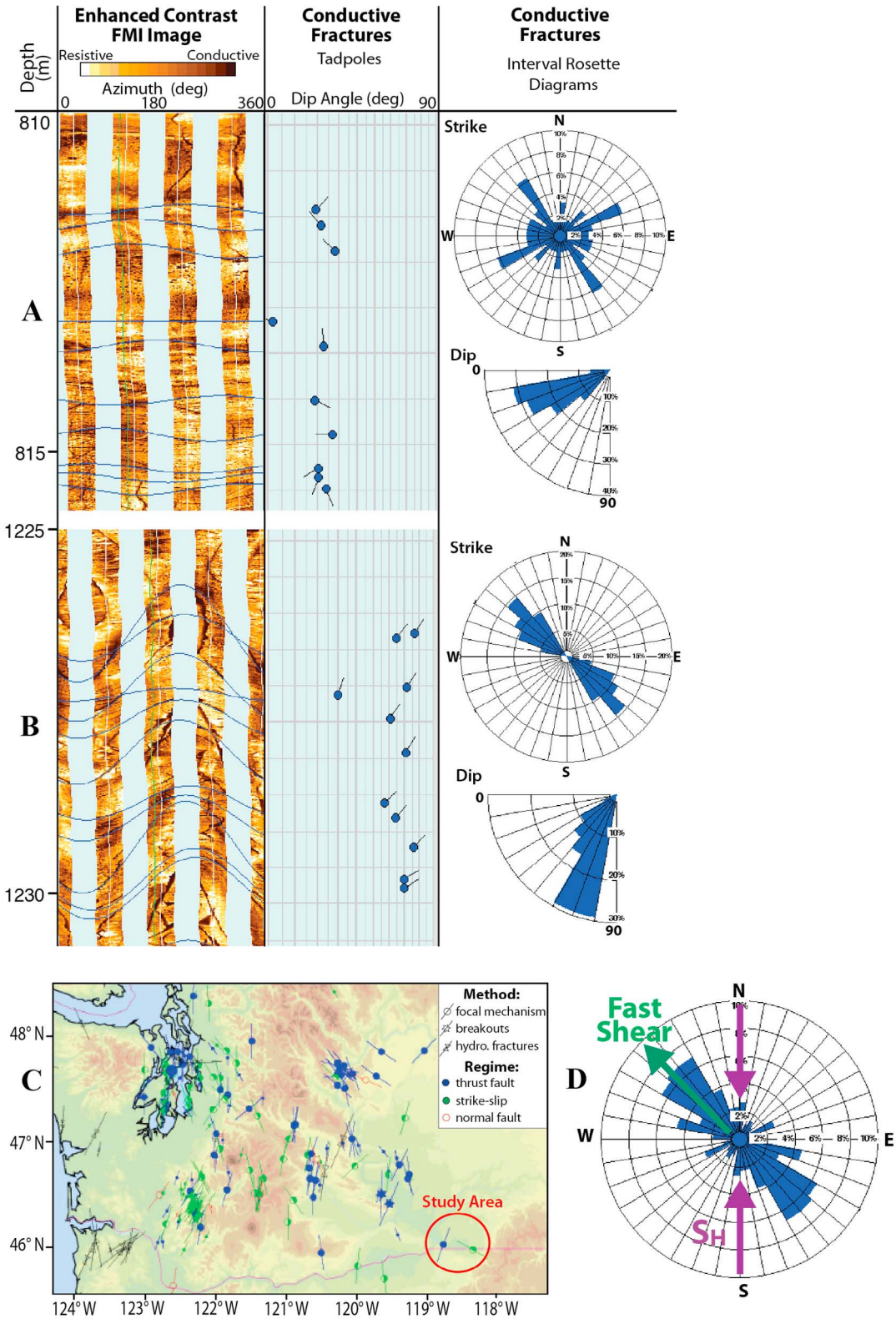

Figure 4. Fracture orientation and stress regime. Examples of (a) sub-horizontal cooling joints and (b) high-angle tectonic fractures interpreted in the Wallula FMI images (shallow dip angles might be overestimated due to visual interpretation bias); (c) stress map for Washington, 0–10 km depth [*Heidbach et al.*, 2008]; (d) the composite diagram of the strike direction for conductive fractures identified in the FMI record (blue), the fast shear azimuth estimated by *Sullivan et al.* [2011] (green), and the inferred direction of the maximum regional horizontal stress from *DOE* [1988] (purple).

with an enlarged borehole diameter, but the low readings cannot be ascribed to borehole size variations alone. The effect of borehole size is generally higher in brecciated zones and in high GR flows, but is about 5–8 API, on average, and never exceeds 15 API. Although the decrease in the GR activity in some brecciated flow tops is of the same magnitude, the GR activity predicted from the core chemistry using tool-specific coefficients [*Ellis and Singer*, 2007] closely matches the corrected GR log both in flow tops and flow interiors (Figure 2). This confirms that the observed GR signal is due to variations in chemical composition of the basalt, and that the borehole effect has been corrected. Higher GR activity could be expected in the brecciated flow tops compared to unaltered flow interiors due to the presence of clay minerals, such as has been reported in altered ocean floor basalts [e.g., *Broglia and Moos*, 1988], but no such pattern is observed in the Wallula logs. On the contrary, altered flow tops often have lower GR activity than unaltered flow interiors. The sample-based GR calculation allows estimation of the relative contributions of K, U, Th, which co-vary in the following concentration ranges: 0.3–2.3 wt%, 1.6–6.1 ppm, and 0.4–1.86 ppm, respectively. Their average relative contributions to the total GR are 39%, 38%, and 23%, and the variation in these elemental concentrations and the associated GR activity are mostly of magmatic origin and appear to be less affected by mineral changes caused by the basalt alteration.

[22] Borehole geochemical logs from the Elemental Capture Spectroscopy (ECS) tool indicate a narrow compositional range for major elements in the Grande Ronde Basalt and a relatively large difference with the Wanapum Basalt (Figure 5). Within the Grande Ronde, Si content varies on average (median $\pm 2\sigma$) within 22–28 wt%, Fe content is 8–11 wt%, Ca content is 3–8 wt%, Ti content is 1–1.5 wt%. The most pronounced changes in chemical composition occur within the Slack Canyon member (790–867 m), which has elevated Ca and low Fe and Ti concentrations, and the other flows do not exhibit significant changes. Mg, Na, Al, and K concentrations estimated from ECS are less reliable due to low contribution of these elements in the neutron capture spectrum. Nonetheless, they provide a bulk estimate for K = 0.5–2 wt%, Al = 4–9 wt%, Na = 1–3 wt%. The Mg concentration has high uncertainty and the estimated bulk concentration of Mg = 0–3 wt% is not reliable.

[23] The continuous chemistry from the ECS logs is in good agreement with chemical analysis of sidewall cores and cuttings, despite uncertainties introduced by inclusion of spectral yields for Mg, Na, Al, and K, and by other neutron absorbers. Table 2 shows that the root mean square difference between XRF analysis on cuttings and ECS logs is less than 1 wt% for all elements except Al (1.08 wt%). The difference with ICP data is slightly higher, exceeding 1.5 wt% for Al and Fe (e.g., three sidewall core samples from brecciated flow tops). In Figure 5, localized discrepancies between core and log data may be due to 2 orders of magnitude or more difference in their volumes of investigation. The ECS estimates may also be influenced by the gamma spectrum stripping process, which may overestimate Fe while underestimating Al, due to the close proximity of their spectral peaks. Given the inherently high Al uncertainty in the ECS results, the log agreement with core and cuttings data is remarkably good. Overall, borehole spectroscopy provides a reliable in situ measurement of the bulk rock chemistry, and these data demonstrate its successful application in a basalt formation.

[24] With the narrow compositional range and high uncertainty in the ECS data, a multivariate statistical analysis was employed to resolve small statistically significant changes and underlying correlations in elemental concentrations. The results of R-mode factor analysis for the 8 ECS logs suggest that 70% of the variance can be explained by only 3 factors. The first factor is a combination of Fe and Ti, which co-vary (Figure 6a); the second most significant factor is influenced by co-varying Ca and Mg, anti-correlated with Na; and the third factor is influenced by Al and Si. Concentration of Ti, mimicked by Fe, show some of the most distinct differences between flows in the ECS log, and therefore, they contribute most significantly to the ECS spectrum. The first factor describes variations in the petrologic content of titanomagnetite and ferrous mafic minerals in the formation. The second factor (related to Ca and Mg) primarily reflects the variability in clinopyroxene content.

[25] Factor analysis for XRF-derived elemental concentrations from both cores and cuttings results in a similar pattern (Figure 6b). Two factors retain 77.7% of the variance. The first factor is a combination of co-varying Ca and Mg versus Na, K, and Si; the second factor reflects Fe and Ti variations. The similarity of variance-covariance matrix structure for the ECS and core data confirms the overall accuracy of borehole spectroscopy and its ability to depict inherent chemical variability for basalt with a narrow compositional range. The comparison also highlights some limitations of neutron capture spectroscopy in basaltic rocks. The variance in XRF

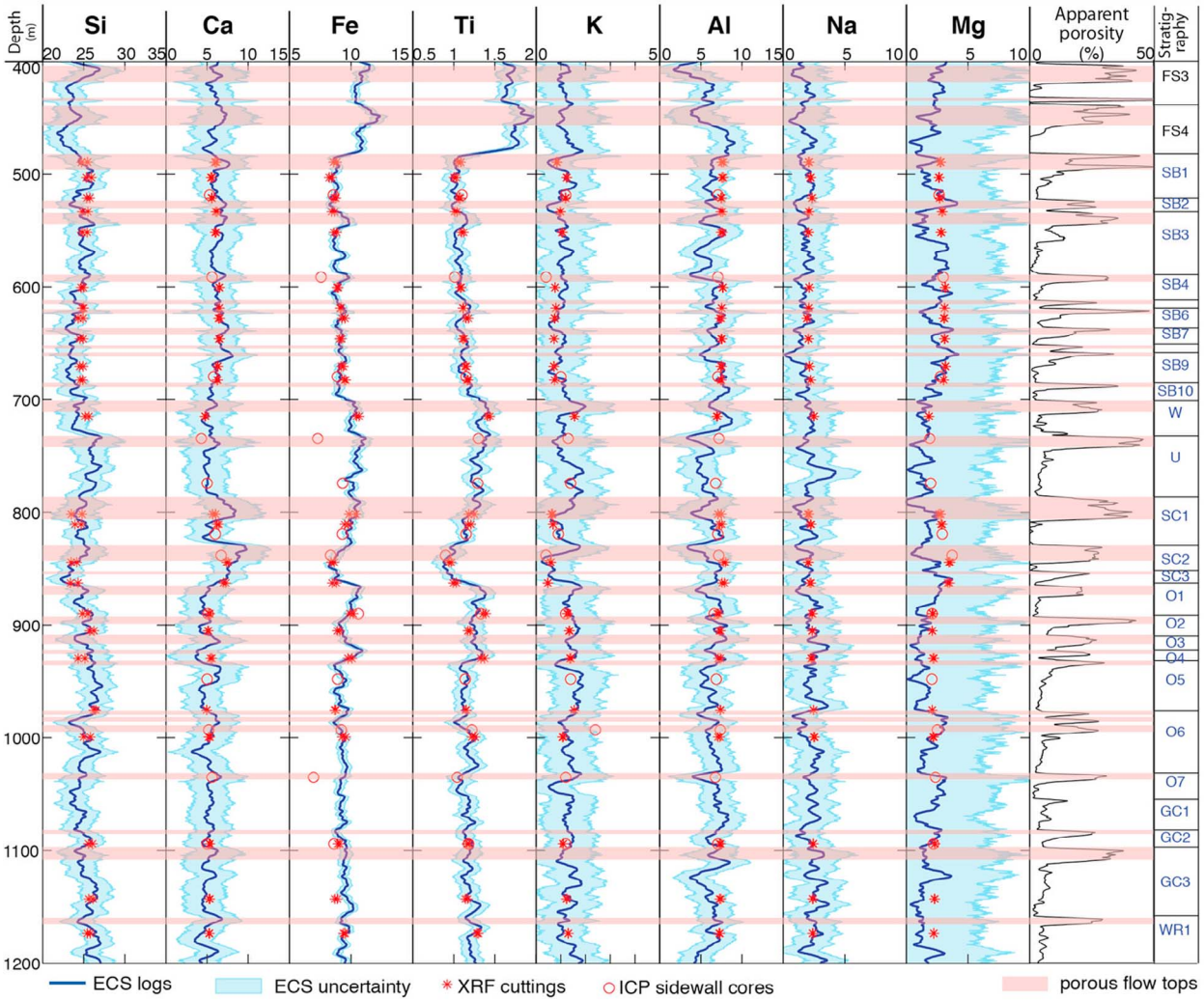

Figure 5. Comparison of the borehole geochemistry logs from Elemental Capture Spectroscopy (ECS) to the chemistry data from sidewall cores and cuttings (in weight %). Highlighted zones (pink) correspond to porous flow tops characterized by extensive mineral alteration.

data is dominated by Ca-Mg and Na-K-Si variability that correspond to clinopyroxene and plagioclase content, respectively, the two major mineral constituents of the CRBG. The ECS logs, however, are more sensitive to Fe and Ti, and dominantly reflect the variability in these two elements, while Ca and Mg factor is pushed into second place, and the Na-K correlation is not clear. However, despite high uncertainty in the elemental yields for Ca, Na and

Table 2. The ECS Statistics: Median Concentration Values for the 8 Measured Elements, the Standard Deviation as a Measure of Variability in the Grande Ronde Formation, the Root-Mean Square Difference (E_{rms}) Between the XRF Measurement on Cuttings and the Corresponding ECS Values, and the Root-Mean Square Difference Between the ICP Sidewall Core Data and the ECS

	Si	Ca	Fe	Ti	K	Al	Na	Mg
ECS_median	24.99	5.57	9.38	1.17	1.21	6.34	2.06	1.71
ECS_stdev	1.72	1.15	0.76	0.13	0.35	1.15	0.63	0.82
E_{rms} cuttings XRF	0.75	0.97	0.52	0.07	0.36	1.08	0.47	0.98
E_{rms} core IPC		1.09	1.55	0.05	0.43	1.71		1.18

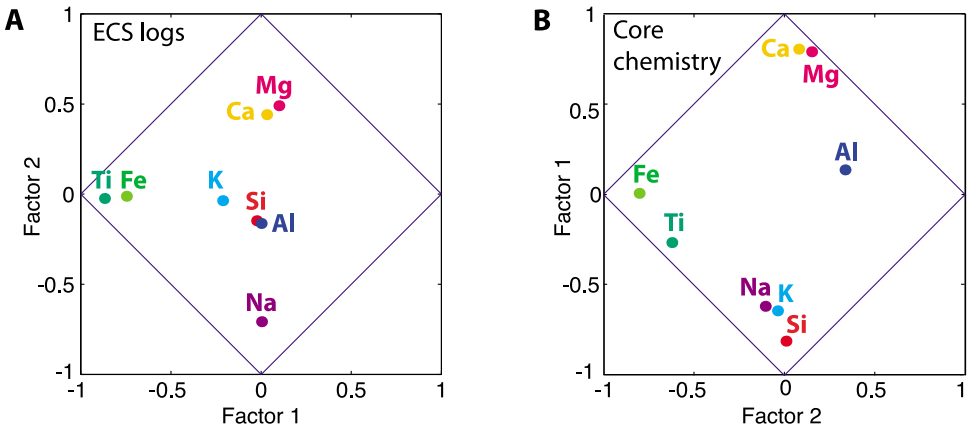

Figure 6. Results of R-mode factor analysis for (a) the Wallula ECS logs and (b) for the same elements from the sidewall core chemistry. The position of points on the plot represents each element's fraction of the total variance associated with the two major factors. The diamond border represents the maximum variance of each variable; therefore, elements plotted near the border have most of their variance explained by those factors.

Mg, the ECS logs correctly depict the statistical relationship between these elements.

5. Discussion

5.1. Borehole Spectroscopy Potential for Mineralization Monitoring

[26] High mineral trapping potential is one of the key advantages of sequestering anthropogenic carbon in igneous rocks, resulting in permanent binding of injected fluid into stable solid phase and providing long-term storage by reduced risk of leakage. Monitoring of in situ carbonate precipitation is therefore likely to become a key aspect of post-injection monitoring of carbon storage in basalt. Direct measurements of mineral content are usually done ex-situ, and require sampling and extensive laboratory analysis. Borehole spectroscopy may provide continuous in situ information about mineral composition, however, if geochemical logs can be converted to mineralogy through a site-specific mineral model of known chemical composition [e.g., *Herron*, 1986]. In order to investigate the sensitivity of geochemical logging to secondary mineralization, we first analyze its ability to detect existing natural alteration in basalt and then extrapolate to the chemical changes expected after carbon dioxide injection.

[27] The Grande Ronde Basalt is characterized by extensive natural alteration in its vesicular flow tops, as observed in all of the sidewall core samples collected from those zones (Figure 2). Their dominant secondary minerals include phyllosilicates (predominantly Fe-rich smectite and celadonite), zeolites (clinoptilolite and heulandite), and silica-polymorphs. Abundances vary from almost zero in unaltered basalt to tens of percent in extensively altered zones [*Horton*, 1991; *Porter*, 2010]. These mineral changes, however, are not clearly manifested in the 8 major and minor elemental concentrations detected by the ECS. Figure 5 indicates no consistent differences in elemental concentrations in flow tops and flow interiors. Chemical analysis of sidewall cores confirms that differences in the mean elemental concentration in flow tops and flow interiors are generally less than the range of chemical variability within each group (Figure 7a). Thus, in terms of the 8 major and minor elements, these fresh-water bearing basalts appear as a closed system. The elements are dissolved from the basalt matrix and are bound by alteration in the proportions similar to the original matrix composition, although their oxidation and hydration states become significantly different (Figure 7b). These alteration products therefore cannot be detected by the ECS. Figure 8 shows that depleted K can be detected in some brecciated zones and elevated Ca/K ratios often correspond to altered zones, but the relationship is not unique. The ratio of (Ca+Mg) to Na (or Na+K+Si) better describes the mafic/silicic mineral content. A chemical alteration index (e.g., Al versus Ca+K+Na) approach does not apply in this environment. Furthermore, none of the elemental ratios derived from the ECS correlate with porosity, which is perhaps the best proxy for brecciated and altered zones. No elemental ratio is uniquely indicative of alteration in the Grande Ronde flows, unfortunately. In part, this result may be explained by alteration variability among the different flow tops, such as observed in the sidewall

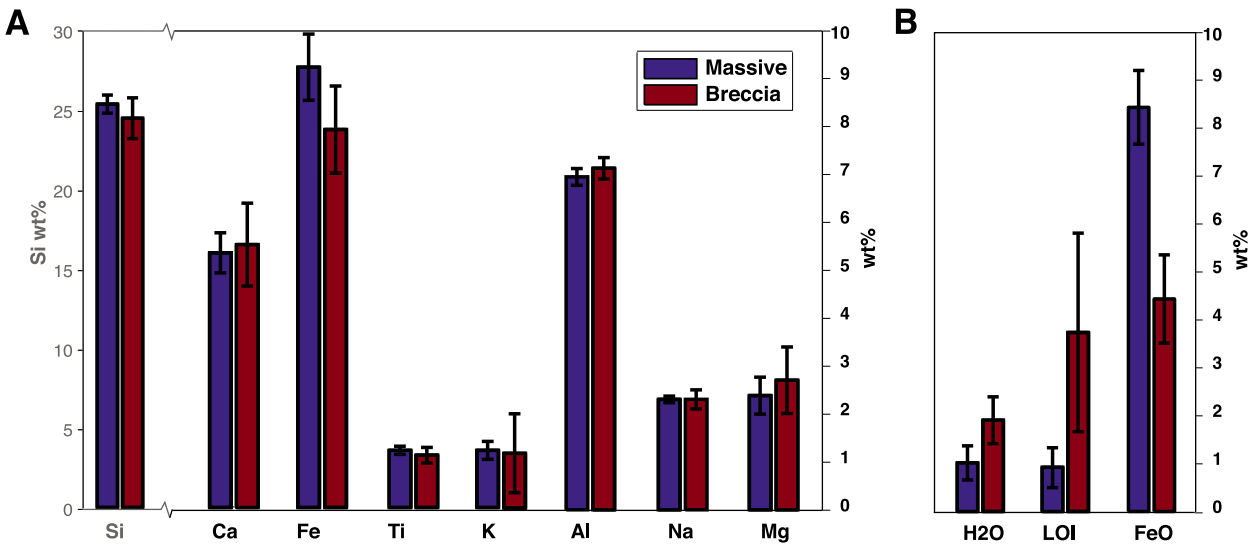

Figure 7. Comparison of the chemical composition of the massive (unaltered) and brecciated (altered) sidewall cores: (a) concentrations of the 8 major and minor elements detectable by the ECS indicate no significant difference between flow tops and flow interiors (Si and Na computed from XRF oxide concentration, all other elements from ICP spectroscopy); (b) volatile content (Loss on Ignition), water content (Penfield), and iron II concentration (Titration) are significantly different in the flow tops and flow interiors. The bar height indicates the mean value for the group, error bars correspond to 1 standard deviation and represent the variability within each group.

cores (e.g., white pore coatings, blue-green pore fillings, oxidized red matrix, etc). Additional data on the mineral content of individual flow tops are needed to better distinguish the matrix and alteration chemistry using the ECS. With a single mineral model, it is not possible to detect the log-derived mineral alteration in the Grande Ronde flows.

[28] While natural alteration is not clearly manifested in the ECS logs, a different set of chemical reactions and alteration products may be expected under the conditions created by a CO_2 injection. Dissolution rates generally increase with decreasing pH and the relative release rates of important carbonate-forming cations may differ. *Schaef and McGrail* [2009] studied the dissolution behavior of CRBG samples over a range of temperatures and solution pH and demonstrated that measured concentrations of Si in solution were higher than for all other cations (Al, Mg, Fe, Ca and Na), regardless of temperature or solution pH. Al, for example, showed the slowest release rate at high temperature and low pH. *Schaef et al.* [2009, 2010] investigated composition of the carbonate precipitates formed within pore space and on the surfaces of individual CRBG grains in the laboratory. After several hundred days of exposure to water and supercritical CO_2, the majority of samples precipitated pure calcite with limited amounts of Fe, Mg, and Mn substitution, suggesting that Ca may be preferentially bound into carbonates formed as a result of CO_2 injection. If in situ CO_2 injection similarly results in a few percent change in Si, Ca, and Fe concentrations in the solid phase, the ECS will be able to detect mineralization, thus, providing a tool for mineralization monitoring using time-lapse borehole spectroscopy. Studies of basalt reactivity under actual in situ conditions are needed to quantify the degree to which carbonation will occur in the CRBG and the resulting detectable changes in major cation concentrations.

[29] High-energy pulsed-neutron logging tools (e.g., Reservoir Saturation Tool™) that collect the full spectral content and are capable of measuring a larger number of elements, including the C/O ratio, may be able to offer greater promise for in situ monitoring of carbonate mineralization. Such pulsed-neutron tools generate neutrons at 14 MeV, and therefore, allow measurement of inelastic interactions, the only detectable source of gamma rays from carbon and oxygen [*Ellis and Singer*, 2007]. Pulsed neutron tools require longer acquisition times, but because the carbon content and C/O ratios would change drastically after a CO_2 injection into these formations, the CRBG may provide an ideal environment to test the applicability of neutron-pulsed tools for long-term geochemical monitoring. Note, however, that distinguishing injected CO_2 in pore spaces from newly formed carbonate minerals

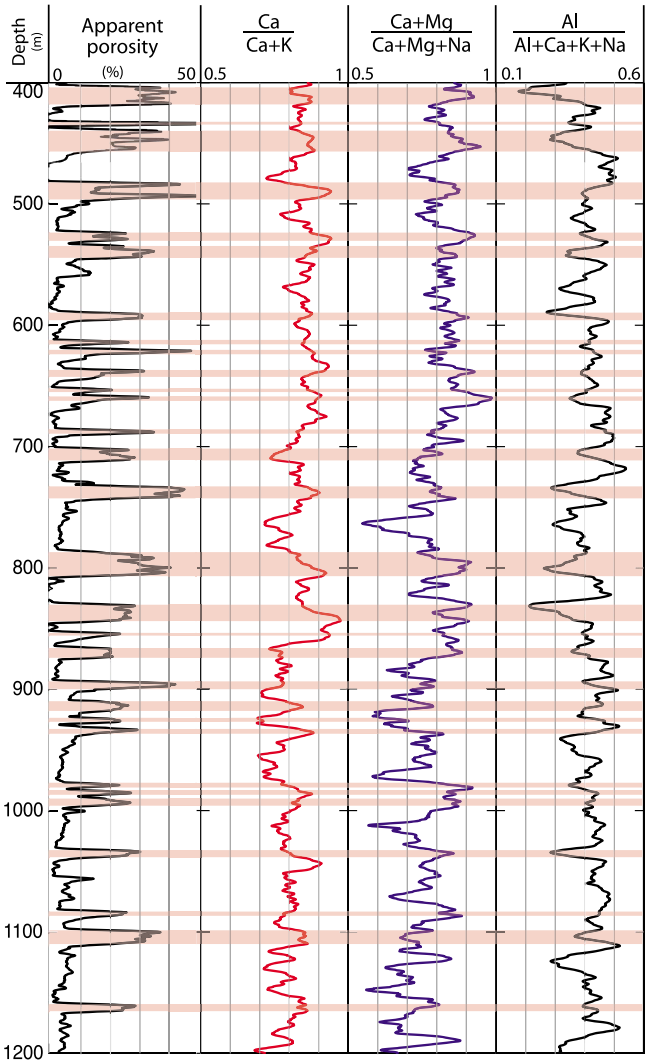

Figure 8. Examples of characteristic elemental ratios from the ECS logs illustrating a lack of pronounced chemical changes in the porous flow tops compared to the massive flow interiors. Highlighted zones (pink) correspond to porous flow tops characterized by extensive mineral alteration.

may be challenging while the injected fluids remain in the test reservoir.

5.2. Reservoir and Sealing Properties of CRBG

[30] The layered CRBG flow sequences offer multiple options for consideration as reservoir and caprock formations (Figure 9). The following section reviews three most important aspects that must be considered for the optimum reservoir identification: specifically, the reservoir hydraulic properties, its mineralization potential, and the caprock integrity. Downhole logging data can contribute significantly to understanding each of these parameters, although of course, data from a single well cannot address the lateral variability of these critical formation properties. Downhole logs can provide an important first step toward understanding the intrinsic properties of the CRBG flows intersected in the Wallula pilot borehole, which may be further considered as reservoirs and caprocks for long-term CO_2 storage.

5.2.1. Reservoir Hydraulic Properties

[31] The two most critical factors determining the quality of an underground fluid storage reservoir is its storage potential (controlled by effective porosity) and its hydraulic conductivity (controlled by permeability). At target depths below 700 m, where CO_2 is expected to undergo supercritical phase transition, geophysical logs in the Wallula pilot borehole indicate at least 13 zones having apparent

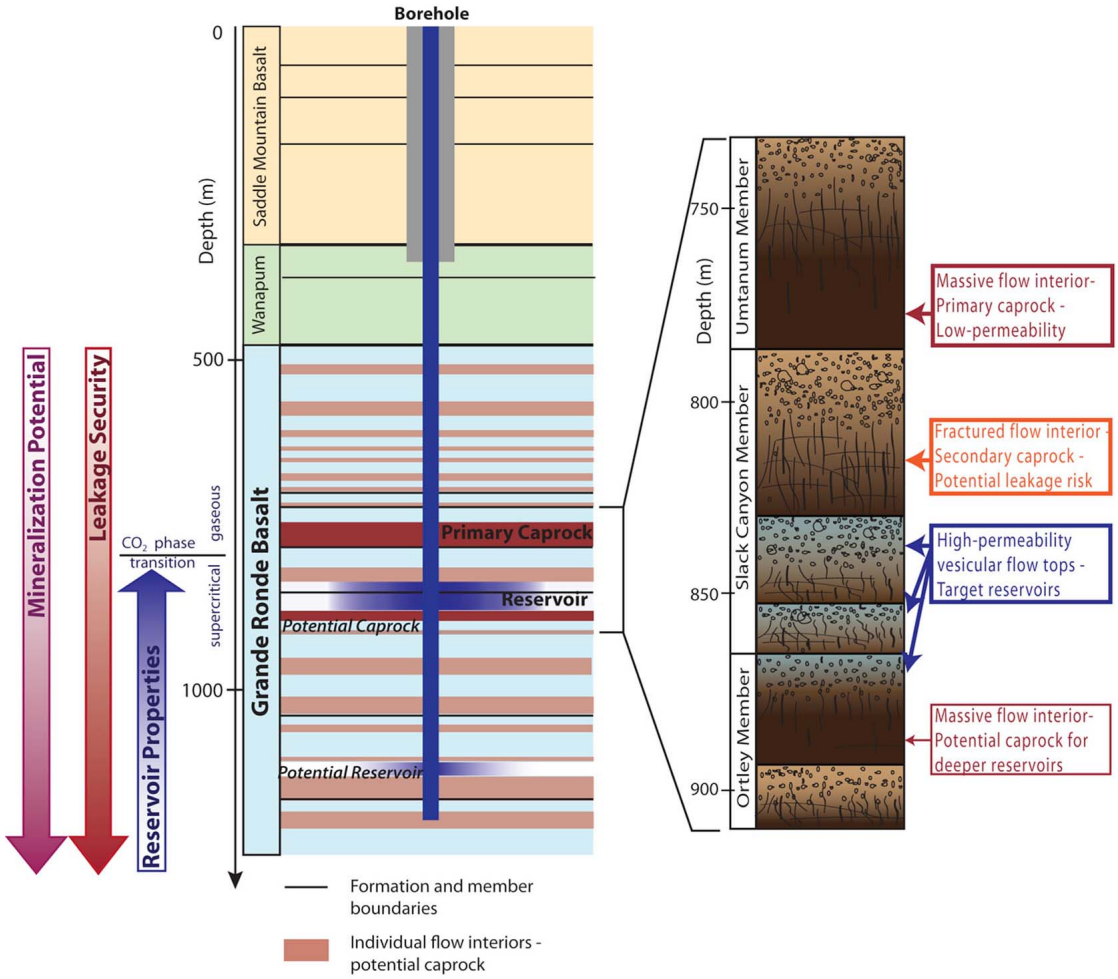

Figure 9. Schematic profile of the Columbia River Basalt intersected by the Wallula borehole, illustrating typical reservoir structure in continental flood basalt with multiple alternating flow interiors (caprock) and interflow zones (potential reservoirs). A structural interpretation of the target injection zone based on the logging data is provided.

porosity over 15%, although only 4 of them exceed 10 m in thickness. *McGrail et al.* [2006] and *Reidel et al.* [2002] previously used the 10 m/15% threshold criteria for evaluating reservoirs. These four are the flow tops of the Umtanum (731–742 m), Slack Canyon 1 (788–808 m), Slack Canyon 2 (830–842 m), and Grouse Creek 3 (1099–1110 m) members of the CRBG (Figure 2). Among the four zones, the Slack Canyon 1 flow top is the thickest, but also highly heterogeneous. All four indicate increases in borehole temperature gradient, suggesting that they may allow fluid inflow/outflow. The deepest Grouse Creek 3 zone is characterized by a much narrow temperature gradient anomaly than the others. Although borehole logs provide clear delineation of these high-porosity zones, the measured porosity is likely to exceed the in situ 'effective' porosity (i.e., the interconnected pore volume available for fluid flow and storage).

[32] The data available for effective porosity in the Grande Ronde Basalt are sparse. Laboratory core analysis at the Hanford Site indicated 7–30% porosity within flow tops [*Loo et al.*, 1984] and 0.1–8.9% within flow interiors [*DOE*, 1988]. These values correspond well with logging results. A more accurate estimate of the effective porosity may be obtained from tracer tests [*Reidel et al.*, 2002]. Two small-scale tracer tests at the Hanford site yielded an extremely low effective porosity on the order of 10^{-4} (i.e., 10^{-2}%) in the McCoy Canyon/Sentinel Bluffs flow top, overlying the Umtanum member [*Leonhart et al.*, 1982]. This member has a 'normal' flow top as opposed to a versicular and brecciated one, however. Hydraulic testing in the Wallula pilot borehole also indicated lower effective porosity in interflow zones than the porosity estimated from logs (F. Spane, personal communication, 2012). Two factors are likely to contribute to this. Clay

infilling of pores and isolated vesicular pores with small pore-throats can both reduce the interconnected porosity available for fluid flow [*Saar and Manga*, 1999]. Logs may therefore not fully or accurately capture the in situ porosity, which underscores the importance of hydraulic testing for porosity estimation in basalt reservoirs.

[33] Hydraulic testing data in the CRBG formations are available at the Hanford Site and in the Wallula pilot borehole. The Grande Ronde Basalt interflow zones typically exhibit a wide range of hydraulic conductivity values, spanning 9 orders of magnitude from 10^{-3} to 10^{-12} m/s and have a geometric mean at 10^{-8}–10^{-7} m/s [*DOE*, 1988]. Measurements of permeability within individual interflow zones in the Pasco Basin show decreasing trends with depth, which is attributed to compaction due to the overburden stress as well as secondary mineral formation [*Spane*, 1982]. Hydraulic testing of 12 conductive intervals in the Wallula pilot borehole was conducted during and immediately after drilling, confirming a similar decrease in hydraulic properties with depth [*McGrail et al.*, 2009]. A decreasing pattern is not reflected in the porosity logs. All of the four high-porosity flow tops (the Umtanum, Slack Canyon 1, Slack Canyon 2 and Grouse Creek 3 members) appear to have elevated hydraulic conductivity values. The Grouse Creek 3 has the highest conductivity among the deepest flows (below the Ortley 1) and hydraulic testing indicated that 90% of the transmissivity in the Slack Canyon 2–3 and Ortley flows (the target injection zone) is localized within the Slack Canyon 2 flow top. *McGrail et al.* [2009] estimated hydraulic conductivity values of (3.8–7.7) $*10^{-7}$ m/s, equivalent to an average intrinsic permeability of 75–150 millidarcies, within the Slack Canyon 2 flow top. The shallowest Umtanum and Slack Canyon 1 flow tops also have high hydraulic conductivity and could be viable reservoirs for injection, if the depth criterion for CO_2 stability in a supercritical state is satisfied.

[34] Quantitative information about lateral variability of the CRBG reservoir properties at Wallula is not available. Previous studies suggested that individual flows and intraflow structures can be laterally continuous for great distances, but the thickness of the flow structures is often variable, controlled primarily by the environment in which they were formed [*Reidel et al.*, 2002]. Earlier studies in the central Columbia Basin [*DOE*, 1988] described instances of both abrupt changes as well as extended lateral continuity in the CRBG flow structures. A seismic reflection survey conducted before drilling the Wallula pilot borehole indicated that no large E-W striking faults associated with the major compressional structures in the Pasco Basin disrupt the 6.5-km N-S trending line at the study site [*Sullivan et al.*, 2011]. More detailed characterization of the lateral heterogeneity of the deep structures could not be resolved from the 2D seismic data. Borehole data from nearby wells are also sparse, but suggest that significant lateral variations in the reservoir properties occur. In particular, a gas exploration well (Shell 1–10 Darcell) located about 30 km northeast from the Wallula pilot borehole intersected a greater number and thicker flow top breccias in the Grande Ronde formation as well as a highly permeable zone at the top of the Wapshilla Ridge member not evident in the Wallula pilot borehole [*McGrail et al.*, 2009]. So, despite the large areal extent of individual Grande Ronde flows, their internal structure may be quite variable and a multiwell study would be necessary to accurately characterize lateral variability within the CRBG.

5.2.2. Mineralization Potential

[35] The long-term behavior of CO_2 injected into basaltic aquifers will be largely controlled by chemical interactions with the formation water and basalt matrix. Mineral trapping provides strong motivation for CO_2 sequestration in basalt and the reservoir chemistry must be considered as an important screening factor in selecting reservoirs with the highest chemical potential, even though the specific geochemical controls on basalt reactivity are not yet fully understood. *Schaef et al.* [2010] compared the chemical reactivity of basalt samples from different volcanic provinces in a series of laboratory experiments with aqueous dissolved CO_2 under supercritical conditions ($scCO_2$). Although basalt reactivity varied considerably, no convincing correlation could be found relating to differences in bulk composition, mineralogy, or glassy mesostasis quantity or composition. Further studies on Wallula borehole cuttings from Grouse Creek member (~1.1 km depth) also considered the effects of reservoir depth and the amount of water entrained in $scCO_2$ [*Schaef et al.*, 2011]. Under pressures and temperatures corresponding to 800–3000 m depths, basalt samples exposed to dissolved CO_2 for identical periods of time appeared to react more vigorously at higher pressures. These observations suggest that deeper basalt flows may be more promising as sequestration targets. Given the observed decrease in hydraulic properties with depth in most cases, a trade-off between favorable hydraulic properties and basalt reactivity is likely to be necessary. Another factor contributing to an

increase in carbonation rate may be related to the presence of secondary minerals, such as chlorite, that enhanced the formation of carbonates in the CRBG samples exposed to water-rich $scCO_2$ [*Schaef et al.*, 2011]. These observations highlight the importance of accurate mineralogical description for predicting in situ mineralization rates.

[36] In terms of the major cation chemistry and mineral speciation, carbonate precipitates from the CRBG samples that reacted with CO_2 are dominated by pure calcite, with limited amounts of Mg, Fe, and Mn substitution [*Schaef et al.*, 2010]. Longer time experiments and higher simulated depth yield more substitutions, and in some cases produced carbonates dominated by Fe-rich species [*Schaef et al.*, 2011]. Reaction products associated with water-rich $scCO_2$ were unique and distinct from the ones forming in aqueous based fluids, and they are not yet as well understood [*Schaef et al.*, 2011]. Overall, the relative predominance of Ca versus Mg may determine which carbonate minerals precipitate, with the more calcic basalts favoring formation of calcite because of its lower solubility [*McGrail et al.*, 2006]. According to the chemical analyses from the ECS and sidewall core data, the highest Ca concentration in Wallula borehole is observed in the Slack Canyon 1 and 2 flow tops, while Ortley 1 and 4 flow tops are characterized by higher Fe content (Figure 5). If elevated concentrations of specific cations accelerate basalt carbonation, continuous geochemical logs may allow identification of the most promising flows for in situ mineralization.

5.2.3. Caprock Characterization

[37] Finally, presence of overlaying flow interior(s) of sufficient thickness and integrity is crucial for identifying a suitable seal to contain a potential CO_2 reservoir. Horizontal hydraulic conductivity from field tests in the CRBG flow interiors range between 10^{-9} to 10^{-15} m/s, with the geometric mean between 10^{-12} to 10^{-13} m/s [*Reidel et al.*, 2002]. These measurements illustrate a similar relationship as flow tops with decreasing hydraulic conductivity with depth. Values for vertical hydraulic conductivity, perhaps the most pertinent to predicting vertical migration of injected CO_2, are very poorly constrained and may be at least an order of magnitude lower [*DOE*, 1988]. Three low-permeability caprock intervals overlying the target injection zone were tested in the Wallula pilot borehole [*McGrail et al.*, 2009]. They are located within flow interiors of the Umtanum member and the Slack Canyon 1 and are characterized by horizontal hydraulic conductivity of 10^{-12}–10^{-13} m/s (i.e., about 0.01–0.1 microdarcies). The flow interior of the Umtanum member is ~40 m thick and provides a regionally recognized low-permeability caprock [*Reidel et al.*, 2002]. Along with the Slack Canyon 1 flow interior, the Umtanum will serve as primary caprock for the target injection zone in the Wallula pilot borehole [*McGrail et al.*, 2009].

[38] An important question for petrophysical characterization is whether any of the logging properties can serve as a proxy for basalt integrity and be used for caprock characterization where hydraulic testing data are limited or not available. Within flow interiors, fractures and joints represent potential compromises to the seal integrity. Borehole images allow for fracture identification as well as quantitative analysis of their abundance and orientation. The presence of fractures does not uniquely correlate with hydraulic properties, as they may be filled or closed [e.g., *Matter et al.*, 2006]. Both Slack Canyon and Umtanum members contain fractured intervals observed in FMI images (Figure 3), but hydraulic testing indicates they have extremely low permeability [*McGrail et al.*, 2009]. Previous studies of the Grande Ronde Basalt cores also showed that joints are generally tight, a high percentage of fractures (77–87%) are completely healed or filled, and most fractures have partial filling or lining of secondary minerals [*DOE*, 1988]. In the CRBG, the presence of fractures or joints does not compromise caprock integrity and generally do not contribute to hydraulic conductivity in the majority of tested flow interiors.

[39] The injection of CO_2 has the potential to alter existing hydraulic properties of fractures by dissolution, mineral precipitation and pressure effects. Understanding of existing fracture networks is therefore crucial in predicting caprock behavior. *Ellis et al.* [2011] studied the evolution of fracture permeability in CO_2-acidified brine flow-through experiments with carbonate caprocks and demonstrated the possibility of very different outcomes for samples from the same formation. One experiment exhibited extensive deterioration along a fracture due to dissolution, while another exhibited a net decrease in fracture permeability due to combination of mineral precipitation and particle clogging. The stark difference in this observed behavior suggests that fracture evolution is highly sensitive to mineral heterogeneity and local variations in flow conditions, and is very hard to predict. Unfractured zones may offer greater long-term caprock security. Borehole images show pervasive fracturing of

basalt flow interiors at the Wallula pilot borehole, but intervals of massive basalt appear to exist at the bottom of certain flows. Zones of massive basalt are thickest in Umtanum and Ortley 1 flows, ~22 m and ~16 m respectively. Qualitatively, electrical resistivity may serve as a proxy for basalt integrity because dry basalt is highly resistive (up to 10^8 Ohm-m), whereas clays and water are conductive and an abundance of open or clay-filled fractures will lower resistivity values. A thorough and quantitative comparison of hydraulic characteristics and resistivities in flow interiors would be necessary before logs could be used for caprock identification. More hydraulic tests and log data within flow interiors in the Wallula pilot borehole could be used to undertake such an analysis.

[40] Taking the advantage of all petrophysical data available in the Wallula pilot borehole, other stratigraphic units in the CRBG that are not targeted for injection in the Wallula project may be studied. Future experiments in continental basalt may be guided by these results and a multiwell characterization of lateral flow heterogeneity would be required to establish the reservoir and sealing properties of any CRBG reservoir at a larger scale. Shallow reservoir zones, such as the Slack Canyon 1 and Umtanum flow tops, have potentially suitable reservoir properties but they occur at the upper threshold of the depth required (about 750 m) for CO_2 to be injected in a super-critical state [*McGrail et al.*, 2009]. Also, no hydraulic data is currently available in the overlying caprock zones. A potential reservoir zone in the Grouse Creek 3 flow top, located at a depth of 1.1-km in the Wallula pilot borehole (Figure 9), has less favorable hydraulic properties but contains a large number of overlying low-permeability flow interiors. If leakage through primary caprock occurred, the longer migration path from this depth may allow for a greater amount of residual trapping and mineralization of dissolved CO_2 before it reaches the surface. The Ortley member may potentially serve as a primary seal for such deeper reservoirs, e.g., the Grouse Greek flows, if deep injection zones were targeted. Overall, deeper sequestration may provide higher sealing security due to fracture closing and a greater number of overlying flow interiors, but the detailed hydraulic properties within deep interflow zones remain unknown.

6. Conclusions

[41] 26 flows from 7 members of the Grande Ronde formation were identified in the Wallula borehole. The flows vary in thickness from 10 to 70 m, with brecciated flow tops about 3–20 m thick and apparent porosity of 20–45%. The majority of the interflow zones have apparent porosity over 15% but only 4 of them uniformly exceed 10 m in thickness: the flow tops of Umtanum (731–742 m), Slack Canyon 1 (788–808 m), Slack Canyon 2 (830–842 m), and Grouse Creek 3 (1099–1110 m) members. The effective porosity of these zones is not well constrained but is expected to be much lower. Interflow zone permeability decreases with depth but is sufficiently high in the shallower flow tops, especially the Slack Canyon 2 (~100 millidarcies).

[42] Flow interiors are pervasively fractured, and are characterized by 0–10% apparent porosity. Natural fractures are broadly classified into low-angle cooling joints (bands) and steeply dipping tectonic fractures. Logging data suggest the Umtanum and Ortley 1 flow interiors may have the largest intervals of highly resistive massive basalt. Although those zones exhibit vein-like fractures in the FMI images, they are interpreted as caused by drilling and confined to borehole walls. The Umtanum and Slack Canyon flows were hydraulically tested and are characterized by extremely low permeability (0.01–0.1 microdarcies) [*McGrail et al.*, 2009]. They are considered the primary caprock in the section.

[43] Custom processing of Elemental Capture Spectroscopy (ECS) logs with formation-specific oxide closure model provides concentrations of 8 major and minor elements in the Wallula borehole (Si, Fe, Ti, Al, Ca, Mg, Na, K) matching sidewall core chemistry data with the average root-mean square error below 1 wt%. The very narrow chemical composition of the Grande Ronde Basalt and limited manifestation of mineral alteration in the bulk chemistry hamper reliable conversion of chemical logs into mineral concentrations. Combined with no spectral sensitivity to carbon, the ECS has limited ability to detect basalt carbonation in fresh-water reservoirs, unless a pronounced preferential release and/or binding of a specific major cation is induced by CO_2 injection. More advanced borehole spectroscopy methods are recommended for CO_2 sequestration monitoring, e.g., high-energy pulsed neutron spectroscopy tools that allow for measuring of inelastic neutron spectrum resulting in increased number of detectable elements, including C/O ratio.

[44] There are numerous high-porosity flow tops in the CRBG which may offer multiple reservoir options. Based on hydraulic test results, the

candidate test injection zone for the Wallula project is positioned between 828 and 887 m and includes Ortley 1, Slack Canyon 2 and 3 flow tops, underlying the Slack Canyon 1 and Umtanum caprock. Deeper reservoirs appear to have inferior hydraulic properties but may offer greater security due to potentially higher mineralization rates, longer leakage migration paths, and larger amount of intermediate caprock. If deep injection zones are considered for CO_2 storage in the Grande Ronde Basalt, the logging data suggest that the Grouse Creek 3 flow top could be a likely candidate reservoir for testing, with the Ortley 1 flow interior as potential primary caprock.

[45] The Grande Ronde flow interiors are characterized by low permeability despite the abundance of fractures, which appear to be closed or filled, and therefore flow interiors represent a caprock. Unfractured massive basalt is much less common in the section, thus, understanding fracture behavior under injection conditions will be the key to evaluating the CRBG sealing properties for CO_2 storage. Ultimately, the interplay between chemical forces of dissolution and mineral precipitation, and the mechanical effects of injection pressure built-up and confining stress will determine the caprock integrity during CO_2 storage, and more studies are needed to address this issue. FMI image analysis combined with results of hydraulic testing is a first step toward understanding of fracture patterns and their properties that can provide information for further modeling and prediction of caprock behavior after a CO_2 injection.

Acknowledgments

[46] The authors gratefully acknowledge the constructive criticisms on the original manuscript offered by Pete McGrail, and especially, Frank Spane, that greatly improved the quality and completeness of the discussion section. Comments from reviewers, in particular, the detailed and comprehensive feedback from Terrence Conlon, were invaluable for improving manuscript's clarity and consistency. The authors would like to thank Marina Polyakov and Alyssa Charsky from Schlumberger Doll Research for help with laboratory analysis. Natalia Zakharova is also grateful to the members of Borehole Research Group at LDEO for insights and useful discussions about well log analysis. TM, mark of Schlumberger.

References

Anderson, R. N., J. C. Alt, J. Malpas, M. A. Lovell, P. K. Harvey, and E. L. Pratson (1990), Geochemical well logging in basalts: The Palisades Sill and the oceanic crust of Hole 504B, *J. Geophys. Res.*, *95*(B6), 9265–9292, doi:10.1029/JB095iB06p09265.

Bachu, S. (2008), CO_2 storage in geological media: Role, means, status and barriers to deployment, *Pror. Energy Combust. Sci.*, *34*(2), 254–273, doi:10.1016/j.pecs.2007.10.001.

Boldreel, L. O. (2006), Wire-line log-based stratigraphy of flood basalts from the Lopra-1/1A well, *Faroe Islands, in Scientific Results From the Deepened Lopra-1 Borehole, Faroe Islands*, *Geol. Surv. Den. Greenl. Bull.*, *9*, 7–22.

Broglia, C., and D. Ellis (1990), Effect of alteration, formation absorption, and standoff on the response of the thermal neutron porosity log in gabbros and basalts: Examples from Deep Sea Drilling Project-Ocean Drilling Program Sites, *J. Geophys. Res.*, *95*(B6), 9171–9188, doi:10.1029/JB095iB06p09171.

Broglia, C., and D. Moos (1988), In-situ structure and properties of 110-Ma crust from geophysical logs in DSDP Hole 418A, *Proc. Ocean Drill. Program Sci. Results*, *102*, 29–47.

Bryan, S. E., and R. E. Ernst (2008), Revised definition of Large Igneous Provinces (LIPs), *Earth Sci. Rev.*, *86*(1–4), 175–202, doi:10.1016/j.earscirev.2007.08.008.

Davis, J. C. (1986), *Statistics and Data Analysis*, John Wiley, New York.

DeGraff, J. M., and A. Aydin (1987), Surface morphology of columnar joints and its significance to mechanics and direction of joint growth, *Geol. Soc. Am. Bull.*, *99*, 605–617, doi:10.1130/0016-7606(1987)99<605:SMOCJA>2.0.CO;2.

Department of Energy (DOE) (1988), Consultation draft: Site characterization plan, reference repository location, Hanford Site, Washington, U.S. Dept. of Energy, Office of Civilian Radioactive Waste Management, *Rep. DOE/RW-0164*, Pac. Northwest Natl. Lab, Richland, Wash.

Dessert, C., B. Dupré, J. Gaillardet, L. M. François, and C. J. Allègre (2003), Basalt weathering laws and the impact of basalt weathering on the global carbon cycle, *Chem. Geol.*, *202*(3–4), 257–273, doi:10.1016/j.chemgeo.2002.10.001.

Ellis, B. R., C. A. Peters, J. P. Fitts, J. P. Nogues, M. A. Celia, M. Dobossy, and A. Janzen (2011), Alteration of caprock fracture geometries during flow of CO_2-acidified brine: Informing basin-scale leakage models from pore-scale modeling and core-scale experiments, Abstract GC42A-08 presented at 2010 Fall Meeting, AGU, San Francisco, Calif., 13–17 Dec.

Ellis, D. V., and J. M. Singer (Eds.) (2007), *Well Logging for Earth Scientists*, Springer, Dordrecht, Netherlands, doi:10.1007/978-1-4020-4602-5.

Goldberg, D. S., and K. Burgdorff (2005), Natural fracturing and petrophysical properties of the Palisades dolerite sill, *Geol. Soc. Spec. Publ.*, *240*(1), 25–36, doi:10.1144/GSL.SP.2005.240.01.03.

Goldberg, D. S., T. Takahashi, and A. L. Slagle (2008), Carbon dioxide sequestration in deep-sea basalt, *Proc. Natl. Acad. Sci. U. S. A.*, *105*(29), 9920–9925, doi:10.1073/pnas.0804397105.

Goldberg, D. S., D. V. Kent, and P. E. Olsen (2010), Potential on-shore and off-shore reservoirs for CO_2 sequestration in Central Atlantic magmatic province basalts, *Proc. Natl. Acad. Sci. U. S. A.*, *107*(4), 1327–1332, doi:10.1073/pnas.0913721107.

Grau, J. A., and J. S. Schweitzer (1989), Elemental concentrations from thermal neutron capture gamma-ray spectra in geological formations, *Nucl. Geophys.*, *3*(1), 9.

GuoXin, L., G. X. YuHua, Z. Jie, Y. FengPing, Y. ChangHai, T. J. Neville, S. Farag, Y. XingWang, and Z. YouQing (2007), Petrophysical characterization of a complex volcanic

reservoir, paper presented at 48th Annual Logging Symposium, Soc. of Petrophysicists and Well Log Anal., Austin, Tex.

Heidbach, O., M. Tingay, A. Barth, J. Reinecker, D. Kurfeß, and B. Muller (2008), *The World Stress Map Database Release 2008*, Comm. for the Geol. Map of the World, Paris, doi:10.1594/GFZ.WSM.Rel2008.

Herron, M. M. (1986), Mineralogy from geochemical well logging, *Clays Clay Miner.*, *34*(2), 204–213, doi:10.1346/CCMN.1986.0340211.

Hooper, P. R. (2000), Chemical discrimination of Columbia River basalt flows, *Geochem. Geophys. Geosyst.*, *1*(6), 1024, doi:10.1029/2000GC000040.

Horton, D. G. (1991), Secondary minerals in Columbia River Basalt, Pasco basin, Washington, *Rep. WHC-SA-1352-FP*, Pac. Northwest Natl. Lab, Richland, Wash.

Intergovernmental Panel on Climate Change (2005), Carbon dioxide capture and storage, special report, Geneva, Switzerland.

Kelemen, P. B., and J. M. Matter (2008), In situ carbonation of peridotite for CO_2 storage, *Proc. Natl. Acad. Sci. U. S. A.*, *105*(45), 17,295–17,300, doi:10.1073/pnas.0805794105.

Lackner, K. S. (2003), Climate change: A guide to CO_2 sequestration, *Science*, *300*(5626), 1677–1678, doi:10.1126/science.1079033.

Leonhart, L. S., R. L. Jackson, D. L. Graham, G. M. Thompson, and L. W. Gelhar (1982), Groundwater flow and transport characteristics of flood basalts as determined from tracer experiments, *Rep. RHO-BWI-SA*, Pacific Northwest Natl. Lab, Richland, Washington.

Long, P. E., and B. J. Wood (1986), Structures, textures, and cooling histories of Columbia River Basalt flows, *Geol. Soc. Am. Bull.*, *97*(9), 1144–1155, doi:10.1130/0016-7606(1986)97<1144:STACHO>2.0.CO;2.

Loo, W. W., R. C. Arnett, L. S. Leonhart, S. P. Luttrell, I.-S. Wang, and W. R. McSpadden (1984), Effective porosities of basalt: A technical basis for values and probability distributions used in preliminary performance assessments, *Rep. RHO-BWI-TI-254*, Rockwell Int. Corp., Richland, Wash.

Martin, B. S., H. L. Petrovic, and S. P. Reidel (2005), *Field Trip Guide to the Columbia River Basalt Group, Goldschmidt Conference 2005*, Pac. Northwest Natl. Lab., Moscow, Idaho.

Matter, J. M., and P. B. Kelemen (2009), Permanent storage of carbon dioxide in geological reservoirs by mineral carbonation, *Nat. Geosci.*, *2*(12), 837–841, doi:10.1038/ngeo683.

Matter, J. M., D. S. Goldberg, R. Morin, and M. Stute (2006), Contact zone permeability at intrusion boundaries: New results from hydraulic testing and geophysical logging in the Newark Rift Basin, New York, USA, *Hydrogeol. J.*, *14*(5), 689–699, doi:10.1007/s10040-005-0456-3.

Matter, J. M., T. Takahashi, and D. S. Goldberg (2007), Experimental evaluation of in situ CO_2-water-rock reactions during CO_2 injection in basaltic rocks: Implications for geological CO_2 sequestration, *Geochem. Geophys. Geosyst.*, *8*, Q02001, doi:10.1029/2006GC001427.

Matter, J. M., W. S. Broecker, M. Stute, S. R. Gislason, E. H. Oelkers, A. Stefánsson, D. Wolff-Boenisch, E. Gunnlaugsson, G. Axelsson, and G. Björnsson (2009), Permanent carbon dioxide storage into basalt: The CarbFix Pilot Project, Iceland, *Energy Procedia*, *1*(1), 3641–3646, doi:10.1016/j.egypro.2009.02.160.

McGrail, B. P., H. T. Schaef, A. M. Ho, Y.-J. Chien, J. J. Dooley, and C. L. Davidson (2006), Potential for carbon dioxide sequestration in flood basalts, *J. Geophys. Res.*, *111*, B12201, doi:10.1029/2005JB004169.

McGrail, B. P., E. C. Sullivan, D. H. Bacon, F. A. Spane, G. Hund, P. D. Thorne, C. J. Thompson, S. P. Reidel, and F. S. Colwell (2009), *Preliminary Hydrogeologic Characterization Results from the Wallula Basalt Pilot Study*, Pac. Northwest Div., Richland, Wash.

McGrail, B. P., F. A. Spane, E. C. Sullivan, D. H. Bacon, and G. Hund (2011), The Wallula basalt sequestration pilot project, *Energy Procedia*, *4*(0), 5653–5660, doi:10.1016/j.egypro.2011.02.557.

McLing, T. L., R. W. Smith, R. K. Podgormey, and J. Taylor (2009), Natural analog CCS site characterization Soda Springs, Idaho implications for the long-term fate of carbon dioxide stored in geologic environments, *Eos Trans. AGU*, *90*(*52*), Fall Meet. Suppl., Abstract H13I-05.

Paillet, F. L., and K. Kim (1987), Character and distribution of borehole breakouts and their relationship to in situ stresses in deep Columbia River Basalts, *J. Geophys. Res.*, *92*(B7), 6223–6234, doi:10.1029/JB092iB07p06223.

Pezard, P. A. (1990), Electrical properties of mid-ocean ridge basalt and implications for the structure of the upper oceanic crust in Hole 504B, *J. Geophys. Res.*, *95*(B6), 9237–9264, doi:10.1029/JB095iB06p09237.

Porter, C. M. (2010), Secondary mineralization in flow tops of Columbia River Basalts: Implication for the sequestration of anthropogenic carbon, BS thesis in Chem.-Geol., Whitman Coll., Walla Walla, Wash.

Raymer, L. L., E. R. Hunt, and J. S. Gardner (1980), An improved sonic transit time-to-porosity transform, in *Transactions of the SPWLA Twenty-First Annual Logging Symposium*, pp. 1–13, Soc. of Prof. Well Log Analysts, Houston, Tex.

Reidel, S. P. (1983), Stratigraphy and petrogenesis of the Grande Ronde Basalt from the deep canyon country of Washington, Oregon, and Idaho, *Geol. Soc. Am. Bull.*, *94*, 519–542, doi:10.1130/0016-7606(1983)94<519:SAPOTG>2.0.CO;2.

Reidel, S. P. (1998), Emplacement of Columbia River flood basalt, *J. Geophys. Res.*, *103*(B11), 27,393–27,410, doi:10.1029/97JB03671.

Reidel, S. P., T. L. Tolan, P. R. Hooper, M. H. Beeson, K. R. Fecht, R. D. Bentley, and J. L. Anderson (1989), The Grande Ronde Basalt, Columbia River Basalt Group; Stratigraphic descriptions and correlations in Washington, Oregon, and Idaho, in *Volcanism and Tectonism in the Columbia River Flood-Basalt Province*, *Spec. Pap. Geol. Soc. Am.*, *239*, 21–53.

Reidel, S. P., V. G. Johnson, and F. A. Spane (2002), Natural gas storage in basalt aquifers of the Columbia Basin, Pacific Northwest USA: A guide to site characterization, *Rep. PNNL-13962*, Pacific Northwest Natl. Lab, Richland, Wash., doi:10.2172/15020781.

Saar, M. O., and M. Manga (1999), Permeability-porosity relationship in vesicular basalts, *Geophys. Res. Lett.*, *26*(1), 111–114, doi:10.1029/1998GL900256.

Schaef, H. T., and B. P. McGrail (2009), Dissolution of Columbia River Basalt under mildly acidic conditions as a function of temperature: Experimental results relevant to the geological sequestration of carbon dioxide, *Appl. Geochem.*, *24*(5), 980–987, doi:10.1016/j.apgeochem.2009.02.025.

Schaef, H. T., B. P. McGrail, and A. T. Owen (2009), Basalt-CO_2-H_2O interactions and variability in carbonate mineralization rates, *Energy Procedia*, *1*(1), 4899–4906, doi:10.1016/j.egypro.2009.02.320.

Schaef, H. T., B. P. McGrail, and A. T. Owen (2010), Carbonate mineralization of volcanic province basalts, *Int. J. Greenh. Gas Control*, *4*(2), 249–261, doi:10.1016/j.ijggc.2009.10.009.

Schaef, H. T., B. P. McGrail, and A. T. Owen (2011), Basalt reactivity variability with reservoir depth in supercritical CO_2 and aqueous phases, *Energy Procedia*, *4*(0), 4977–4984, doi:10.1016/j.egypro.2011.02.468.

Schlumberger (1989), *Log Interpretation: Principles and Applications*, Schlumberger Educ. Serv., Sugar Land, Tex.

Spane, F. A. (1982), Hydrologic studies within the Pasco Basin, paper presented at National Waste Terminal Storage Program Information Meeting, U.S. Dep. of Energy, Richland, Wash.

Spane, F. A., B. P. McGrail, E. C. Sullivan, D. S. Goldberg, T. L. McLing, R. S. Weeks, and R. W. Smith (2007), Big Sky Regional Carbon Partnership - Field Activity Plan: Characterization test for CO_2 sequestration in the Columbia River Basalt Group, report, Pac. Northwest Div., Richland, Wash.

Sullivan, E. C., B. A. Hardage, B. P. McGrail, and K. N. Davis (2011), Breakthroughs in seismic and borehole characterization of Basalt sequestration targets, *Energy Procedia*, *4*(0), 5615–5622, doi:10.1016/j.egypro.2011.02.551.

Tolan, T. L., S. P. Reidel, M. H. Beeson, J. L. Anderson, K. R. Fecht, and D. A. Swanson (1989), Revisions to the estimates of the areal extent and volume of the Columbia River Basalt Group, in *Volcanism and Tectonism in the Columbia River Flood-Basalt Province*, *Spec. Pap. Geol. Soc. Am.*, *239*, 1–20.